Proceedings of
2001 ASME International Mechanical Engineering Congress and Exposition
November 11-16, 2001, New York, NY

IMECE2001/DE-25112

ABUTMENT HAMMERING TOOL FOR DENTAL IMPLANTS

John O'Callaghan, Jr.
Northeastern University

Robert Birichi
Northeastern University

Timothy Goddard
Northeastern University

John Jagodnik
Northeastern University

Sean Westbrock
Northeastern University

ABSTRACT

One method for installing dental prosthetics uses components fastened with a tapered interference fit. An abutment is fastened into an implant to provide an anchor for the prosthesis. The current method of installation involves hammering with a dental mallet, which provides inconsistent force. A proposal to replace this method is presented. The mechanics of the taper lock were examined to determine the optimal seating force. The chosen design was analyzed for potential weaknesses. A proof of concept prototype was fabricated and a prototype is being manufactured for further analysis. Experimentation indicates that the variance of applied force is significantly reduced.

INTRODUCTION

This paper reports on the design of a device to be used in conjunction with the taper-lock abutment system, which is used for prosthetic reconstruction of damaged teeth. In this system, a titanium implant (See Figure 1) is placed in the jaw and bone heals around the implant to anchor it. An abutment, which serves as a post for cementing a prosthetic tooth, is placed in the implant through a taper lock mechanism, which is a tapered interference fit used for affixing the two components. The current method of application involves placing a blunt mechanical punch against the abutment and tapping the end of it with a dental mallet. The force created by the mallet is inconsistent and can lead to insufficient retention force. The inconsistency in this procedure creates a need for a device that will apply a consistent seating force, install the abutment in one application and be versatile for different areas of the mouth.

NOMENCLATURE

a	Implant inner diameter
b	Implant outer diameter
D	Abutment outer diameter
δ	Insertion length
$\bar{\delta}$	Non-dimensional insertion length
d_{pin}	Diameter of hinge pin
d_{shaft}	Diameter of shaft
dh	Differential segment height
dr	Differential segment radius
$d\theta$	Differential segment arc angle
dV	Differential segment volume
E	Young's Modulus
F_1	X component of force on hinge pin
F_2	Y component of force on hinge pin
h	Cement sample height
H	Fixture drop height
K_f	Stress concentration factor
K_t	Notch geometry constant
L_{pin}	Length of hinge pin
L_{post}	Abutment post length
L_{seg}	Segment length
P	Magnitude of force vector in hinge pin
q	Notch sensitivity
R	Segment radius
t	Trigger Ring Thickness
$\sigma_{n,max}$	Maximum normal stress
$\bar{\sigma}_{n,max}$	Non-dimensional maximum normal stress
$\sigma_{pin,max}$	Maximum stress in the hinge pin
$\sigma_{r,max}$	Maximum radial stress
$\bar{\sigma}_{r,max}$	Non-dimensional maximum radial stress
$\sigma_{shaft,max}$	Maximum stress in shaft
$\sigma_{shaft,max,real}$	Real maximum stress in shaft
$\sigma_{shaft,yp}$	Shaft yield point stress
$\sigma_{\theta,max}$	Maximum tangential stress
$\bar{\sigma}_{\theta,max}$	Non-dimensional maximum tangential stress
σ_{yield}	Yield stress
u_h	Expansion in implant segment
u_s	Compression in abutment segment
U	Strain energy
$U_{Abutment}$	Abutment strain energy
$U_{Implant}$	Implant strain energy

PROJECT OBJECTIVES AND REQUIREMENTS

Goals

This project has two goals. The first goal is to analyze the taper lock mechanism used to seat the mating components in order to obtain the required installation force as a function of the abutment insertion depth and retention force. The second goal of this project is to create a tool to deliver this required force consistently and accurately.

Design Requirements

The following are required for the success of the design:

- Due to the space constraints and user comfort, the length, weight and clearance of the tool from the tip of the abutment to the top of the tool will be taken into consideration.
- The tool should accommodate a precision grip to allow control over tool placement.
- The concept chosen will be ergonomic and withstand autoclaving.

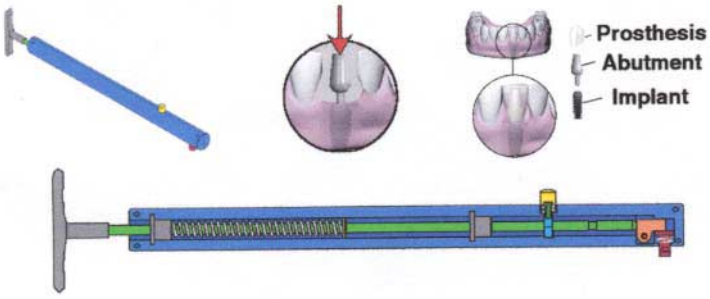

Figure 1: The Taper-Lock System and the Proposed Design

TAPER-LOCK ANALYSIS

To satisfy the first goal of this design, the optimal seating force must be established to optimize the output of the tool. This was achieved through experimentation, finite element analysis and an analytic model.

Experimental Analysis

The taper lock system was evaluated by experimental testing in order to relate the abutment insertion energy to the insertion length (see Figure 2). Insertion length is directly related to the impact energy given to the abutment during impact by the tool and contributes to determining the amount of force required to remove the abutment (retention force).

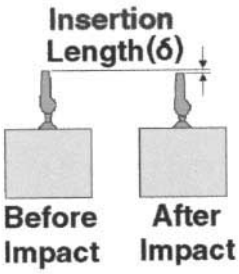

Figure 2: Insertion Length

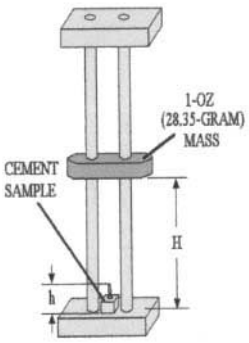

Figure 3: Test Setup

A fixture was designed to relate input (potential) energy to the insertion length (See Figure 3). Varying the drop height "H" determines the potential energy and is related to kinetic energy at impact through an energy balance of the system. Implants were cured vertically into 2 cm cement cubes (cement and bone have similar properties) [1], [2]; insertion length was found by measuring the change in the height "h". A graphical representation of the results is shown in Figure 4.

Note that the non-dimensional parameter $\bar{\delta}$ is given in terms of insertion length (δ) and the length of the abutment post (L_{post}) by:

$$\bar{\delta} = \frac{\delta}{L_{post}} \tag{1}$$

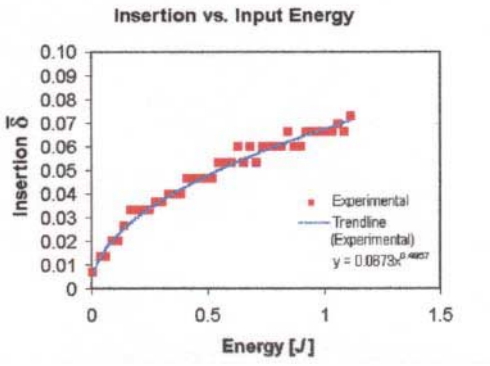

Figure 4: Experimental Insertion vs. Input Energy

FEA

Finite Element Analysis (FEA) using ANSYS version 5.6 was performed on the model to relate insertion length to the stresses in the abutment and implant and to validate stress versus insertion length calculations [3]. Stresses were examined for $\bar{\delta}$ from 0.006 to 0.080. An example is shown in Figure 5. The maximum stresses were found to be below the yield stresses for these insertion lengths.

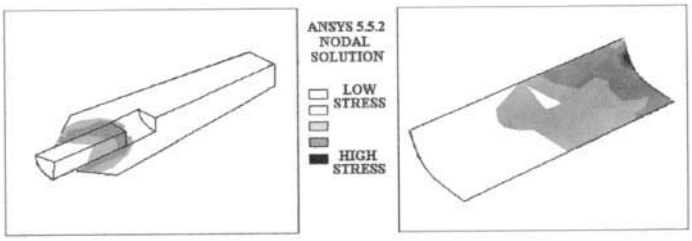

a) Assembly View

b) In depth Inspection of Abutment Post

Figure 5: FEA of Principal Stresses ($\bar{\delta} = 0.080$)

Analytical Model:

To properly evaluate the taper lock mechanism, a model is needed to describe the following:

- The maximum stress within the implant and abutment for a given insertion length.
- The relationship between input energy and insertion length.
- The relationship between abutment retention force and input energy.

Discussion of the Analytical Model:

The basic concept of the model approximates the abutment and implant as a series of independent stacked disks (see Figure 6) that can be analyzed with basic press fit equations. The total strain energy for one step was found by summing the energy to press each disk in a depth equal to the thickness of one disk. This process was then iterated to obtain the required strain energy for a given insertion depth. The model uses 144 disks of uniform thickness to obtain the results (shown in Table 2).

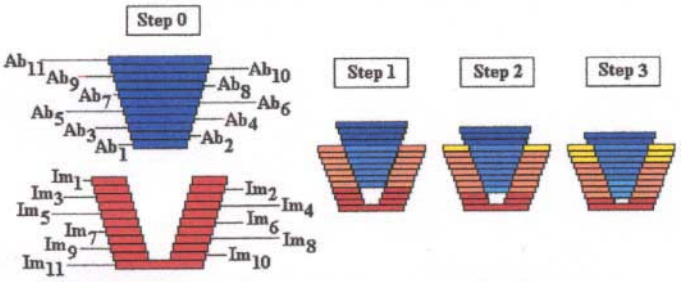

Figure 6: Abutment and Implant Stacked Disk Approximation

Development of the Model

Relation of Strain Energy to Stress

To analyze the segments, the strain energy must be found for each disk. This can be done by treating the segments as controlled volumes and deriving the strain energy equation for each [4]. Strain energy is related to radial and tangential stress and strain by the following:

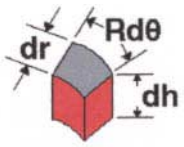

Figure 7: Differential Volume

$$U = \iiint(\sigma_r\varepsilon_r + \sigma_t\varepsilon_t)dV \qquad (2)$$

Where the differential volume (dV) is the product of the differential height (dh), differential circumferential length (Rdθ) and the differential radius (dr) (see Figure 7).

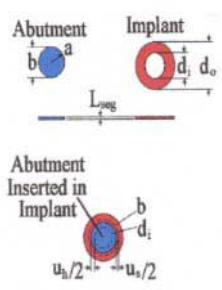

Figure 8: Interference Fit Variables

After substituting boundary conditions and basic press fit equations into equation 2, the integral is performed from a to b to obtain:

$$U = \left[\left(\frac{2.\pi.L_{seg}}{E}\right)\left(\frac{a^4p^2}{(b^2-a^2)^2}\right)\right]\left[\frac{b^4-(a+u_h)^4}{(a+u_h)^2}\right] \qquad (3)$$

Where U is the strain energy, p is the contact pressure and the remaining terms are dimensional variables as defined in Figure 8. This equation is used to compute values for the individual implant segments [5-7].

Application of Strain Energy:

The compression of the abutment post (u_s) and the expansion of the implant (u_h) are related to one another and are a function of stress, friction, contact pressure between the two, material properties and the dimensions of the system. From u_h and u_s, stress and strain can be derived and used to determine the strain energy in each component:

$$U_{Abutment} = \left(\frac{E.\pi.L_{seg}\,b}{4}\right)\left(\varepsilon^2_{t.abutment} + \varepsilon^2_{r.abutment}\right) \qquad (4)$$

$$U_{implant} = \left(\frac{2.\pi.L_{seg}\,a^4p^2}{E(b^2-a^2)}\right)\left(\frac{(a+u_h)^4-b^4}{(a+u_h)^2}\right) \qquad (5)$$

Total strain energy is simply the sum of strain energy over all of the iterative steps. Since work is non-conservative, the work for any step is dependent on the work of all the iterative steps preceding it. These two terms relate to the retention force and required input energy for a given insertion depth.

Results:

Analysis of Jawbone Fracture:

The jawbone was treated as a thick walled pressure vessel that does not the support the implant but experiences pressure when the implant expands during installation. The model predicts a maximum stress, which produces a factor of safety of approximately 10 against jawbone fracture. Fracture is unlikely based on material properties of bone [1], [2].

Impact Stress

The impact energy delivered to the jawbone and abutment must be less the maximum impact that materials involved can withstand (see Table 1) [5]. From the data presented, it is apparent that all of the materials will be able to absorb the input energy without material failure within a factor of safety of approximately 4.

Table 1: Material Properties

Material	Charpy Impact Strength
6Al-4V Titanium	0.548 J
316 Stainless Steel	3.245 J
Human Bone	0.008 J

Stress versus Insertion Length:

The stresses on a differential volume of each component are shown in Figure 9 and the results are shown in Table 2. Note that the maximum normal stresses and maximum shear stresses are obtained from a Mohr's circle analysis that is incorporated in the model and all yield stresses have a factor of safety of 1.5 in order to produce working stresses.

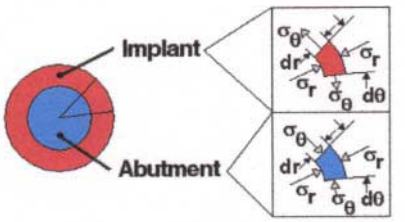

Figure 9: Radial and Tangential Stresses

Table 2: Stress from the Analytical Model

Insertion ($\bar{\delta}$)	$\bar{\sigma}_{n,max}$ (Normal Stress)	$\bar{\sigma}_{t,max}$ (Shear Stress)	$\bar{\sigma}_{r,max}$ (Radial Stress)
0.044	0.436	0.271	0.250
0.052	0.515	0.319	0.295
0.059	0.592	0.366	0.340

The following graph (Figure 10) shows the comparison between the tangential stresses and the insertion length. As can be seen, both analytical methods show that the stresses are acceptable for $\bar{\delta}$ (as defined in equation (1)) under approximately 0.075. Note that the non-dimensional stress $\bar{\sigma}_{\theta,max}$ is given by:

$$\bar{\sigma}_{\theta,max} = \frac{\sigma_{\theta,max}}{\sigma_{yield}} \quad (6)$$

Where $\bar{\sigma}_{\theta,max}$ is the non-dimensional maximum tangential stress, $\sigma_{\theta,max}$ is the calculated tangential stress and σ_{yield} is the yield stress. $\bar{\sigma}_{r,max}$ (radial stress), $\bar{\sigma}_{t,max}$ (shear stress) and $\bar{\sigma}_{n,max}$ (normal stress) are defined similarly.

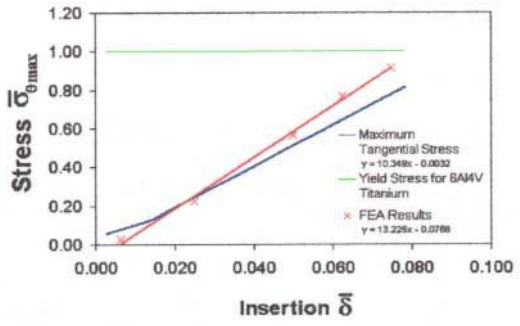

Figure 10: Maximum Tangential Stress versus Insertion Length

Input Force vs. Deflection

As validation of the experiment described above, the insertion length vs. input energy was analyzed in this model, as depicted in Figure 11.

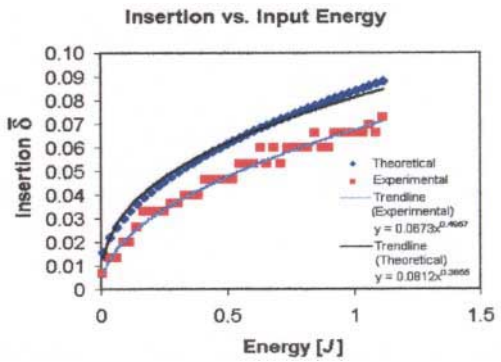

Figure 11: Insertion Length versus Input Energy

The results from the model are a slight over-approximation compared to the experimental results. Frictional losses in the fixture appear to be the main cause for this error. The input energy corresponding to the optimal insertion length is determined Figure 11 and is used in the design of the device.

Retention Force vs. Input Energy

The theoretical model is also able to predict a retention force for a given input energy. From the required energy that relates to the desired insertion length, the retention force was found to be acceptable based on expected forces in the mouth from biting and tooth interaction [8].

TOOL DESIGN

Design Concepts

Once it was determined (through a patent and literature search) that no current technology satisfied the needs of this design [9-17], a solution was conceptualized. The design concept was divided into two sections: methods of applying a single actuating force and methods to redirect the force.

Force Application

The application of force relies on the power source chosen. For single actuating devices, the main concepts focused around four power sources: electric, pneumatic, hydraulic and mechanical. Because of temperature sensitivity and patient safety, only pneumatic and mechanical devices suit the needs of the design.

Force Redirection

A major objective of the design was to find a way to redirect the force perpendicular to the force vector of the power source. After analyzing different design concepts, a hinged piece was decided upon. A shaft will hit this hinge, which will rotate

around a pin and strike a hammering component perpendicular to shaft (see Figure 14).

Evaluation Criteria

After conceptualizing multiple designs for force application and redirection, the proposed solutions were evaluated through the following phases to determine the optimal design.

- Functionality and safety
- Reliability of the critical components of each design
- Manufacturability
- Ease of assembly and ease of use
- Analysis of benefits

Choice of Design

After analysis, two design concepts remained that would provide a solution to the problem presented. The mechanical design (*pull back knob mechanism*; see Figure 12b) was chosen over the pneumatic design (*pneumatic with button*; see Figure 12a) because of concerns over o-ring wear and lubrication, handle sealing issues and its dependency on an external power source (such as an air compressor)

a) Pneumatic with Button b) Pull Back Knob Mechanism

Figure 12: Proposed Designs

Recommended Design Concept

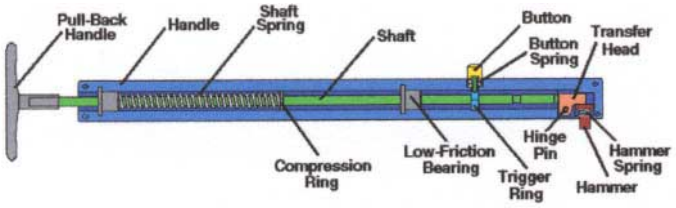

Figure 13: Recommended Design Concept

The final design consists of 19 components as shown in Figure 13. The springs and (4) handle screws are made from 316-medical-grade-stainless steel, the low friction bearings are made from a Teflon impregnated polymer and the remaining components are made from a medical grade titanium alloy (Ti6Al4V).

The tool is a two-stage device. During the first stage, the user pulls back on the pullback handle causing the shaft spring to be compressed between the handle and the compression ring attached to the shaft. The spring-loaded trigger ring and pulls up into a groove on the shaft to lock it in place.

In the second stage, the button is pressed, the ring falls out of the groove and the compressed shaft spring pushes the shaft forward. The shaft impacts the transfer head, which transfers the force perpendicular to the shaft and into the spring-loaded hammer. The hammer protrudes from the tool and transfers the energy directly into seating the abutment. The hammer is threaded to allow the tool to be adapted to accommodate different size abutments.

Analytical Investigations

Spring Selection

The springs of this design are based on the required energy, stress, fatigue and availability of each. The button spring was selected based on anthropomorphic data of acceptable button pushing forces [18]. The shaft spring was selected based on a deflection of approximately 1 cm to produce the required input energy. Finally, the choice of the hammer spring was based on the weight of the hammer and the required force to return the spring to its original position after impact.

Hinge Pin Analysis

The hinge pin, depicted below in Figure 14, is subject to an impact force.

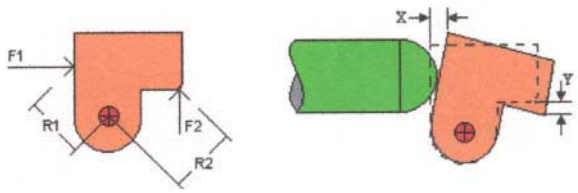

Figure 14: Hinge Pin Analysis

Treating this system as a simply supported beam, the maximum moment is found in relation to the forces acting on the pin. From this, the maximum stress can be related to the pin dimensions. The maximum stress in this component is:

$$\sigma_{pin,max} = -\frac{PL_{pin}\left(d_{pin}/2\right)}{12\left(\pi.d_{pin}^4/64\right)} = -\frac{8PL_{pin}}{3*\pi*d_{pin}^3} \quad (7)$$

Where P is the resultant force of F_1 and F_2 and L_{pin} and d_{pin} are the length and diameter of the pin respectively. Calculations show that the maximum stress in the pin is 434.634 MPa. This is within a factor of safety greater than 2 given the tensile yield stress of 880.434 MPa. The shaft imposes a shear stress of 48.290 MPa, which is below the 550 MPa ultimate-shear stress for this material [5].

Trigger Ring Analysis

The mechanics of the trigger mechanism are depicted in Figure 15. The shear force on the ring can be calculated using simple geometry and elementary shear force equations. Note that the shaft is only in contact with a small portion of the arc length of the shaft as shown in Figure 16.

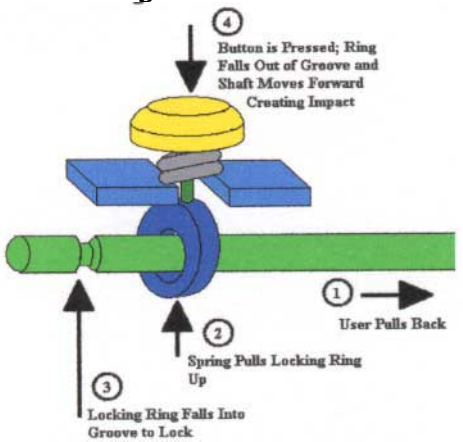

Figure 15: Trigger Mechanism

The thickness of the trigger ring (t) was chosen as 0.25 cm based on space limitations. This creates a shear stress value of 2.38 MPa, which is below the maximum allowable shear stress for stainless steel [5].

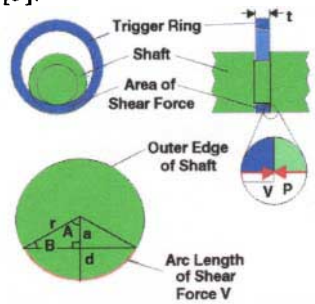

Figure 16: Analysis of Trigger Shear

Shaft Analysis

Groove Shearing

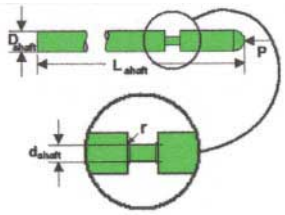

Figure 17: Analysis of the Shaft Groove

The groove in the shaft must be analyzed in order to reduce the chance of the groove wearing down over time. Stress is given in terms of the variables defined in Figure 17 as:

$$\sigma_{shaft,max} = \frac{4P}{\pi . d_{shaft}^{2}} \quad (7)$$

To account for the grove, the real maximum stress is governed by:

$$\sigma_{\substack{shaft, \\ max \\ real}} = K_f \sigma_{shaft,max} \quad (8)$$

Where K_f is the stress concentration factor given by:

$$K_f = 1 + q(K_t - 1) \quad (9)$$

The variable q (notch sensitivity) is assigned a value of 0.57 based on a worst-case scenario for the fatigue in the groove. K_t is tabulated as 2.7 [6]. Using these values, the real maximum stress ($\sigma_{max, real}$) is calculated as 17.68 MPa. Since this is below the yield point stress ($\sigma_{shaft, yp}$=206.90 MPa), the factor of safety is found to be 11.7 against yield.

Fatigue

Using standard fatigue analysis on a shaft with cyclic linear motion, the shaft has a calculated factor of safety of 14.1 against fatigue (based on fatigue analysis discussed in *Machine Design*) [6].

Shaft Buckling

The shaft has a 0.01 cm deep groove to capture the compression ring during loading (based on the required snap ring groove depth), which reduces the effective diameter to 0.15 cm. The critical load was calculated as 154.21 N. From this, a value of 22.24 MPa was calculated for the critical stress, which is considerably less than the compressive yield stress of titanium (1.07 GPa). The actual force seen by the shaft is approximately 17.8 N, which provides a factor of safety of 4.8 against buckling and allows the shaft to be made of readily available stock.

Dynamic Effects

The Model

A vibration model has been developed to show how the shaft and transfer head behave with relation to one another during use. Treating the system as a spring-mass-damper system, iteration was performed over small increments of time to obtain the results presented. The results of the model are shown graphically in Figure 18.

First, the shaft (dashed line) is shown just after the button has been pressed. The shaft quickly obtains a terminal velocity before it comes in contact with the shaft. A short time later, the shaft comes in contact with the transfer head (bold line), changing its initial velocity, as depicted by the change in slope of the dashed line.

When the shaft initially impacts the transfer head, there is a transfer of momentum resulting in a semi-elastic collision. The transfer head accelerates away from the shaft at an almost constant velocity. For a short period of time, the transfer head remains stationary since its momentum is being balanced by the energy in the hammer spring. The components then return to

their initial positions. The model approximates the hammering action to occur at less than 0.005 seconds.

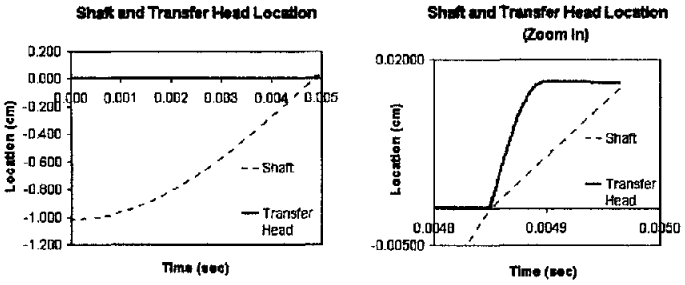

Numerical Results:

In the model, the shaft hits transfer head at 0.00485 seconds. At 0.00490 seconds, the transfer head fully inserts abutment. In this time interval, the tool moves a maximum of 0.0019 cm forward. This creates an angle of 0.04° with relation to the abutment and 0.07% of the energy will go into shearing energy, which is negligible.

Linear Bearings

After initial design, polymer self-lubricated bearings were found to aid in reducing losses from kinetic friction. These bearings are made of a Teflon-impregnated temperature-resistant polymer and are lightweight, autoclavable, and fit well in the small diameter handle.

Weight

For user comfort, the design is required to weigh less than 2.22 N. Based on current projections, the approximate weight of the tool is 1.21 N.

FURTHER DESIGN CONSIDERATIONS

Proof of Concept

Figure is a representation of the proof of concept prototype that was built, which allows testing of the design. The model is a double-scaled model of the design but is a good representation of the mechanics of individual components.

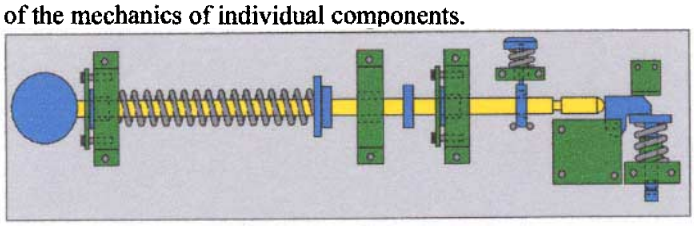

Figure 19: Proof of Concept Design

Experimental Testing

Consistency

A practitioner was consulted to show the consistency of the current method. The dentist performed the procedure on 19 implant samples using the current tooling. Insertion depth was measured for each sample with a sensitivity of 0.00254 cm. For comparison, the proof-of-concept prototype was tested in a similar manner.

Results of Consistency Testing

The results of this testing are shown in Figure 20.

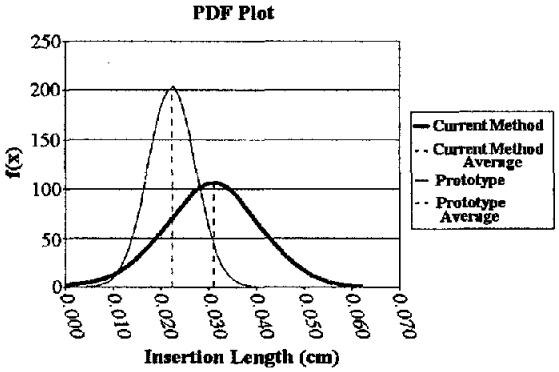

Figure 20: Results of Consistency Testing

The bold lines represent the current method; the thin lines indicate the prototype consistency. Note the improved consistency over the current method as indicated by the taller, thinner peak.

Further Testing

After the prototype has been manufactured, further testing should be performed to ensure the safety and consistency of this design. See the recommendations section below for more detail on further testing.

Other Considerations

Regulatory

This device is classified as a Class 1 device, meaning that it is an accessory to non-invasive surgery [19], [20]. Mechanical power eliminates the need to comply with many regulations, including 501k- pre-market approval.

Industrial Design

One of the goals in the handle design is to maintain a straight wrist. The dental profession is highly susceptible to repetitive motion nerve damage, such as carpal tunnel syndrome. The common method of holding a dental tool is with a precision grip (as shown in Figure 21), which allows control over the placement of the tip inside the mouth [21]. The button is placed to accommodate this type of grip. Other ergonomic issues should be examined during subsequent revisions of the handle design.

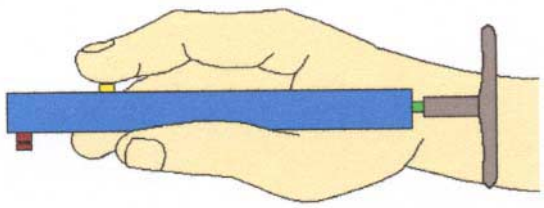

Figure 21: The Precision Grip

Economics

A preliminary cost analysis shows that this tool is reasonably inexpensive to manufacture. A non-binding quote indicates a cost of $70 per unit for 1000 units.

RECOMMENDATIONS

Further testing is recommended before release of this device to the public. Autoclave cycling should be performed to evaluate the effects of thermal stresses during sterilization. Drop testing and cyclic testing should be performed in order to analyze the failure of the device. Accelerated aging will provide another scale for endurance of the tool. Clinical tests to show the consistency of the method in standard use are also recommended.

CONCLUSIONS

The chosen design has been analyzed and shows significant improvements over the current method. The force redirection allows the tool to be versatile in all areas of the mouth. The output of the device takes into consideration the optimal input energy as determined through a mathematical model, experiments and finite element analysis. The goal of relating input energy to insertion length and retention force has also been satisfied. Components of the device were designed to reduce failures due to stresses and fatigue. The double-scale prototype was tested and indicates that the design will satisfy the goal of improved consistency over the current method.

ACKNOWLEDGMENTS

Special thanks goes to Associate Professor Sinan Muftu of Northeastern University for his role of academic advisor for this design project.

REFERENCES

[1] Evans, F. Gaynor. Mechanical Properties of Bone, by F. Gaynor Evans. Pp. 83-121. Springfield, IL. Thomas [1973]

[2] The Complete Sculptor, Inc. FGR-95 Hydrocal. Online. Internet. Available: http://www.sculpt.com/catalog_98/ CastingMaterials/GYPSUMS/gypsum11.htm [Viewed September 14, 2001]

[3] ANSYS User's Manual, Swanson Analysis Systems, Inc. Houston, PA [1992]

[4] Shigley, Joseph Edward. Mechanical Engineering Design. 2nd ed. Pp. 73-83. New York: McGraw-Hill [1972]

[5] Hibbeler, R.C. Mechanics of Materials. 3rd ed. pp. 452-480. Upper Saddle River, New Jersey: Simon & Schuster [1997]

[6] Spotts, Merhyle Design of Machine Elements. 6th ed. pp. 548-553. Englewood Cliffs, NJ: Prentice Hall [1985]

[7] Roark, Raymond J. Roark's Formulas for Stress and Strain. 6th ed. pp. 259-273. New York: McGraw-Hill [1989]

[8] Martin, Rick, The Power of Shark Bites. Online. Internet. Available: http://www.elasmo.com/martin/bite.html. [Last Viewed September 14, 2001]

[9] Lee, G., Hydraulic hammer having improved seal ring, U.S. Patent no. 6,119,795, September 19, 2000.

[10] Bates, L.G, Electrically Operated Hand Tool, U.S. Patent no. 1,772,852, [June 8, 1927]

[11] Hopkins, E.L., Power Operated Pick Hammer for Sheet Metal Work. U.S. Patent no. 2,714,918, [August 9, 1955]

[12] Hufnagel, F.M., Angularly Operable Head for Impact tools, U.S. Patent no. 3,286,558, [November 22, 1966].

[13] McShirley, R. C., Electrical Dental Mallet, U.S. Patent no. 3,921,044, [November 18, 1975].

[14] Wagner, W. R., Abutment Delivery System, U.S. Patent no. 6,099,311, [August 8, 2000].

[15] Harris; J. M., Electric stapler, U.S. Patent no. 6,135,337, [January 15, 1999].

[16] Ilagan; A. M. Electric nailing gun, U.S. Patent no. 5,941,441, [March 10, 1998].

[17] Mukoyama; K. Pneumatic tool, U.S. Patent no. 6,145,727, [November 14, 2000].

[18] Sanders, M. and McCormick, E. Human Factors In Engineering Design. 7th ed. McGraw-Hill Inc. [1993]

[19] U.S. Food and Drug Administration, HHS Publication FDA 95-4158, Premarket Notification 501(k): Regulatory Requirements for medical devices [August, 1995] http://www.fda.gov/ cdrh/manual/510kprt1.html [Viewed September 14, 2001]

[20] U.S. Food and Drug Administration, Recognition and Use of Consensus Standards. Online. Internet. [June 20, 2001]. Available: http://www.fda.gov/cdrh/modact/ k982.html [Viewed September 14, 2001]

[21] Givens, David B, "Precision Grip" [April 2001]. Online. Internet. http://members.aol.com/nonverbal2/precise.htm [Viewed September 14, 2001]